MODELLING OF CORE CRUSH PHENOMENON DURING THE PROCESSING OF HONEYCOMB SANDWICH PANELS

Sanesh Iyer[1], Lucie Riffard[1], Tara Baker[2], Marta Elleby[2], Pascal Hubert[1]
[1]McGill University
Department of Mechanical Engineering
Montreal, QC H3A 0C3, Canada
[2]The Boeing Company
Boeing Research & Technology
Ladson, SC 29456, USA

ABSTRACT

Autoclave co-curing of carbon-fibre prepregs and Nomex honeycomb sandwich structures reduces the number of manufacturing apparatus and time required, presenting clear cost advantages. However, the application of pressure and viscous nature of prepregs can cause motion of the core during processing, leading to scrapped parts. In this work, a finite element model which predicts the occurrence of core-crush is developed and used to study the effect of various processing and geometric parameters on the core crush phenomenon. The effects of prepreg curing are considered in the development of this finite element. The friction behaviour of prepregs as well as the in-plane elastic and plastic properties of honeycomb cores are measured experimentally. The permeability of prepreg is measured experimentally to determine pressure inside the core during cure. The finite element model is validated against experimental data and is shown to accurately predict the onset of core crush for 81% of evaluated cases. The material contained in this paper is based upon work supported by NASA under award No. NNL09AA00A and 80LARC17C0004.

Keywords: Honeycomb core, crush, modelling
Corresponding author: Pascal.hubert@mcgill.ca

SAMPE neXus Proceedings. Virtual Event, June 29 – July 1, 2021. Society for the Advancement of Material and Process Engineering – North America.

1. INTRODUCTION

The manufacturing of composite sandwich structures can involve several manufacturing defects. Among them, core crushing as shown in Figure 1 involves the collapse of the honeycomb core (HC) caused by the pressure applied in the autoclave. The occurrence of core crush depends on the pregreg, adhesive and core properties, panel geometry, bagging conditions and cure cycle. Several authors have studied this phenomenon experimentally and found that the internal core pressure and prepreg friction behaviour significantly influenced core crush [1-4]. Even though HCs are widely used in aerospace applications, measurement and modelling of HCs are still active fields of development. As a result, there are several assumptions and simplifications which will have to be made to model the core crush phenomenon.

Measurement standards focus on sandwich structures which include HCs (see [5, p. 3]) can be adapted to study the HC itself, as was the case for this work. Herein lies the first challenge, with a lack of experimental techniques it is difficult to measure properties for the modelling of HCs. HC behaviour in the in-plane [6] and out-of-plane [7] directions can be derived analytically, in theory enabling an extrapolation from the solid-material behaviour to that of an HC structure made of those materials. Complicating this is the fact that some HC studied in this work is a Nomex-Phenolic composite itself, made by dipping Nomex paper in phenolic resin. As noted by Roy et. al. [8], the behaviour of a HC is sensitive to processing parameters and has to be calibrated for specific core manufacturing methods. Notable process variations include the number of phenolic dips and the cure cycles used. Given the sensitivity of HC properties to interactions of geometry and manufacturing processes, it's important that mechanical properties are measured directly on the HC of interest, and not made from solid-model extrapolations.

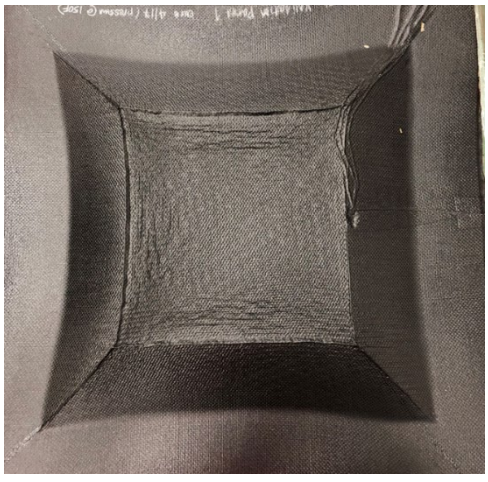

Figure 1 Example of core crush observed on composite sandwich panels cured in an autoclave.

For finite-element modelling – both for in-plane and out-of-plane cases – the explicit modelling of the honeycomb structure is the prevailing technique (see [9-13] for examples). The honeycomb structure can be modelled with continuum shell (S), continuum solid shell (CSS), or continuum solid (CS) elements. The core-skin interface cannot be represented using S elements due to their infinitesimal edges and can be using CSS and CS elements. However, this adds further

computational complexity as it requires a very fine mesh for core and the skin. It is also possible to represent the honeycomb using an equivalent solid mesh (ESM) using CS elements with constitutive models for material properties such as Mohr & Doyoyo's [14]. ESM requires fewer elements and is thus the most computationally efficient option which allows for the evaluation of core skin contact. ESM, however, cannot capture large compressive strains correctly. Furthermore, the core-skin interface must be carefully studied to ensure contact is accurately homogenized as the apparent continuous surface is not representative of an actual honeycomb.

As both experimentation and modelling of honeycomb cores are not mature, the objective of this paper was to develop a model for sandwich panel core crush during manufacturing as a function of specifically defined part geometry, materials, bagging and cure conditions.

2. MATERIAL CHARACTERIZATION

The sandwich panel skin materials studied in this work consisted of carbon fibre epoxy (Hexcel 8552-1) and a toughened epoxy resin prepreg system designed for out of autoclave manufacturing (CYCOM 5320-1) bonded to the core with FM309-1. Nomex HRH-10-1/8-3.0 (3.175 mm cell size) and Nomex HRH-10-3/8-3.0 (9.525 mm cell size) honeycomb core from Hexcel are used. The cure kinetics and viscosity models were available directly from the open source materials library in RAVEN [15] from Convergent Manufacturing Technologies.

2.1 Skin permeability

A test matrix was defined in order to investigate the effect of skin geometry, air evacuation strategy and processing parameters on skin air permeability evolution during cure. More specifically, the varying parameters are listed in the Table 1 below.

Table 1. Parameters defining the skin permeability test matrix.

Parameter	**Levels**
Permeability direction	In-plane, transverse
Honeycomb cell size	3.175 mm, 9.525 mm
Skin material	Cycom 5320-1, Hexcel 8552-1
Skin ply count	thin, medium and thick (Cycom 5320-1); thin and medium ply count (Hexcel 8552-1)
Cure cycles	cycle 1 and 2 (Cycom 5320-1); cycle 3 (Hexcel 8552-1)
AFP compaction pressure	200 N, 667 N

The permeability measurement fixture consists of an aluminum frame with a cavity that encloses the honeycomb core (Figure 2 a)). The core dimensions are 75 mm X 150 mm a thickness of 25 mm. Once the honeycomb is placed in the cavity, one ply of adhesive film and the epoxy skin was placed on the core. The system was vacuum-bagged, and a vacuum pump was connected to the core cavity, along with a valve and a vacuum regulator allowing to control the pressure in the cavity. A flowmeter and a pressure sensor were connected to the bag. The core pressure, the bag pressure, the air flow, and the temperature was monitored during the cure. For in-plane permeability, a non-perforated release film was used on top of the skin and the two longest edges

were sealed with tacky tape. For transverse permeability, a perforated release film was placed on top of the skin and all four edges of the skin were sealed with tacky tape.

The skin air permeability, K (m^2), was calculated from the measured core (P_{core}) and bag (P_{bag}) pressures and the air flow (Q) recorded by the flowmeter during the cure.

$$K = \frac{Q\mu l}{SdP} \quad [1]$$

where Q is the air flow (m^3/s), μ is the air viscosity (Pa.s), dP is the pressure gradient between the core and the bag (Pa) or $dP = P_{core} - P_{bag}$, S is the flow cross section (m^2) and l is the characteristic flow length (m). Figure 2b) shows the flow cross section and characteristic length for a transverse and in-plane permeability measurement.

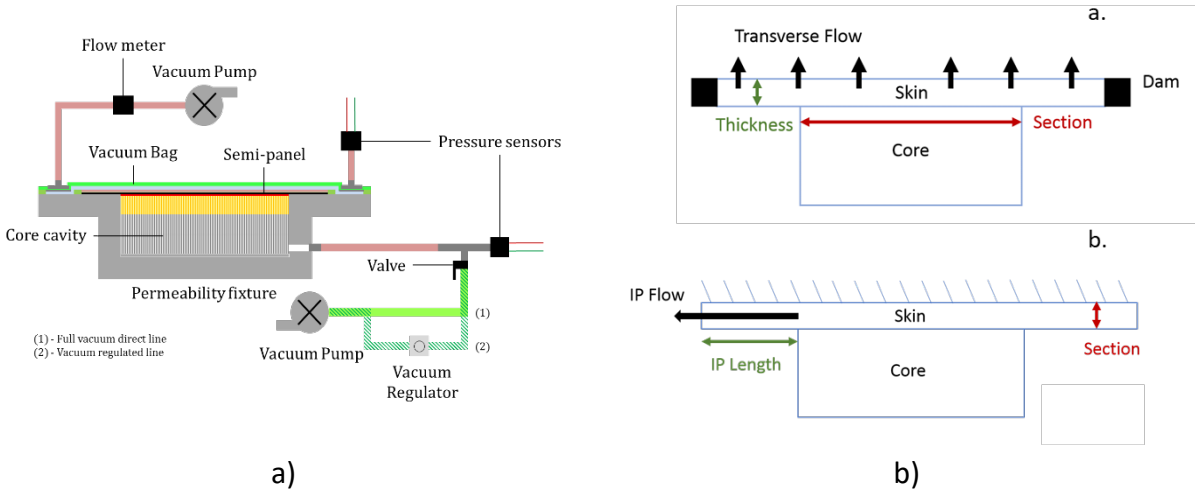

Figure 2 a) Permeability fixture instrumentation and sample layup, b) Dimensions definition for transverse (a.) and in-plane (b.) permeability calculation.

Typical permeability trends are displayed in Figures 3 and 4, focusing here on the Cycom 5320-1 samples. The Hexcel 8552-1 skins manufactured by AFP exhibit almost the same permeability trends as Cycom 5320-1 skins. Figure 3 shows the effect of core cell size on the evolution of the skin air transverse and in-plane permeability for cure cycle 2. Figure 4 shows the effect of skin ply thickness on the evolution of the skin air transverse and in-plane permeability for cure cycle 2.

First, the core cell size does not affect the skin permeability. Moreover, for both Cycom 5302-1 and Hexcel 8552-1 samples, the skin air permeability fluctuates during the resin liquid phase and stabilizes after gelation. It is also clear that in-plane permeability is higher compared to transverse permeability. Interestingly, the skin thickness has inconsistent effect of transverse permeability as 12 plies skin is more permeable than 6 plies skin, which is not logical. In contrast, the Hexcel 8552-1 skin thickness does not have a significant effect on skin permeability. AFP compaction pressure does not have a significant effect on skin permeability either.

Skin permeability was computed and averaged for the different testing conditions, until gelation of the resin. The permeability values are compiled in Table 2. These results are consistent with data found in the literature for plain weave out-of-autoclave prepregs; $5.0x10^{-17}$–$7.8x10^{-17}$ for transverse permeability and $3.8x10^{-15}$–$1.1x10^{-14}$ for in-plane permeability [16]. For simplicity and based on the observed trends, these calculated values of skin permeability can be used for core pressure modelling purposes.

It is worth mentioning that some of the permeability data was inconsistent, probably due to the uncertainty in the experimental procedure, more particularly the sensitivity of the sample sealing conditions. The experimental method is being refined and improved.

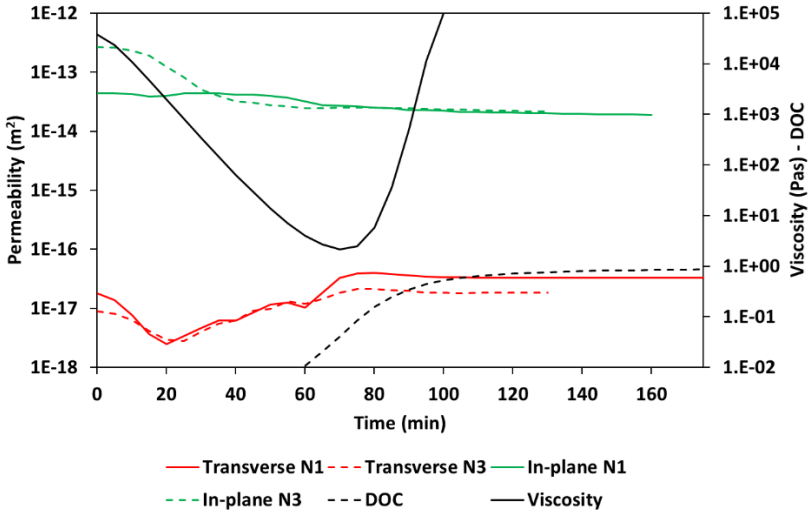

Figure 3 Effect of core cell size (N1 – 3.175 mm, N3 – 9.525 mm) on transverse and in-plane permeability for Cycom 5302-1 and cure cycle 2.

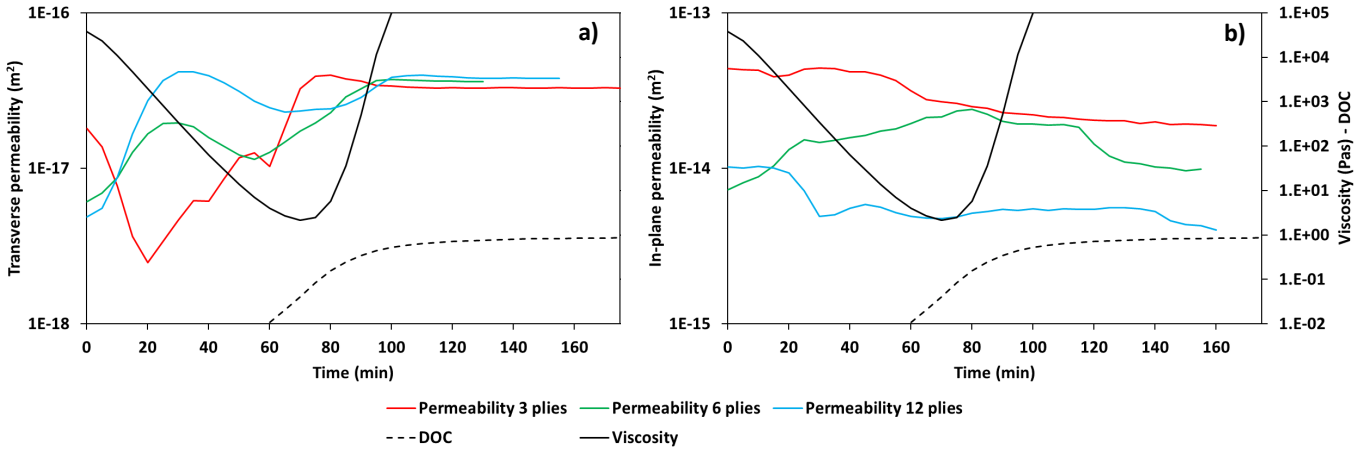

Figure 4 Effect of ply thickness on a) transverse and b) in-plane permeability for Cycom 5302-1, 3.175 mm core and cycle 2.

Table 2 Calculated average skin permeability for Cycom 5320-1 and Hexcel 8552-1.

		Cycom 5320-1	**Hexcel 8552-1**
Permeability (m^2)	Transverse	1.60×10^{-17}	1.19×10^{-17}
	In-Plane	2.96×10^{-14}	2.35×10^{-14}

2.2 Core compression tests

Experimental data which measured the compressive behaviour of stabilized and honeycomb cores is used to define the linear elastic stiffness and yield stresses for different core configurations and orientations. The compression tests were performed on a universal testing frame fitted with rigid parallel plates (Figure 5a)) with test matrix as shown in Table 3. The core samples were cut to length and width of 25 mm X 25 mm and 75 mm X 62 mm for the 3.175 mm and 9.525 mm core respectively. A linear regression is used, where the slope of the linear region is used as the modulus and the first stress which deviates from the target R^2 value, shown in Figure 5b).

Two tests are conducted for each configuration, so an average value of the two tests is used, shown in Figure 6. Using these experimental results, the effects of cell size and core thickness on material properties can be studied. From Gibson et. Al. [6] it is not expected that there is variation in in-plane properties due to core height, but it is experimentally observed. For unstabilized cores, the fact that there is up to 40% variation in experimental results indicates that there is an issue with the test apparatus and experimental methods. There appears to be an even greater variation due to core height in stabilized samples. The increase in variation is partially explained by the fact that stabilization occurs only at the surface, so the core height will influence it. It is also possible that inconsistency in the stabilization process contributes to the measurement error.

Table 3 Parameters defining the core compression test matrix.

Parameter	**Levels**
Material direction	Ribbon (11), Transverse (22)
Honeycomb cell size	3.175 mm, 9.525 mm
Core thickness	thin, thick
Core stabilization	Non stabilized, stabilized

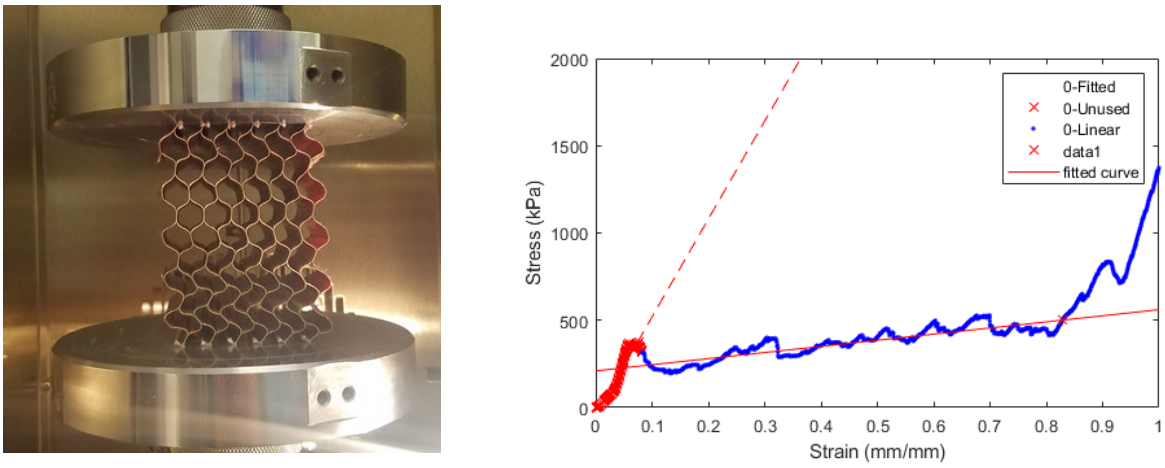

a) b)

Figure 5 a) Core compression test fixture, b) Representative core compression stress strain curve showing the elastic region (red) and collapse region (blue).

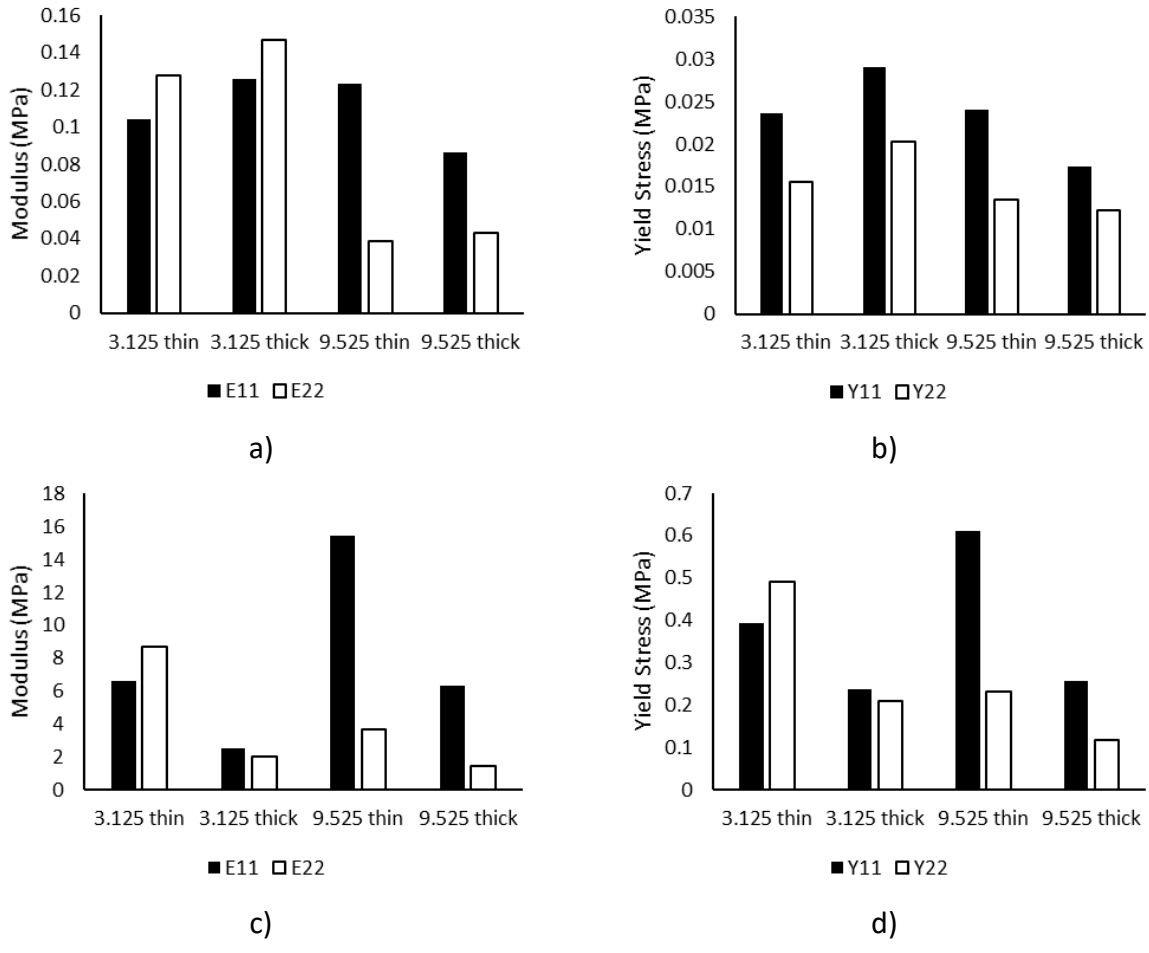

Figure 6 Core compression test data summary, a) Non stabilized modulus (E), b) Non stabilized yield stress (Y), c) stabilized modulus, d) stabilized yield stress.

Looking at cell size, it is expected that there is a performance difference between the 3.125 [mm] and 9.525 [mm] cores as per Gibson et. Al. [6]. It is observed that there is significant effect of core cell size and the in-plane properties for stabilized samples. Addressing the quality of experimental results, it can be expressed in percent variation between the two tests done for both modulus and yield stress in each in-plane direction for each core configuration. For both modulus and yield stress there is significant variation in the results, up to above 500%. The variation appears to be bigger for stabilized samples, indicating further study needs to be done on the effects of processing variables on the core stabilization process. The experimental results indicate that the stabilization process is significantly affected by both core height and core cell size. The observed variability in experimental results indicate that more characterization should be done, especially relating to the stabilization process. For the finite element model, orthotropic properties are required. To calculate these, Ashby & Gibson's formulae are evaluated with the experimental data [6].

2.3 Skin friction

The interply prepreg friction coefficient was measured on a testing setup developed at the McGill Structures and Composite Materials Laboratory (Figure 7 a)). Large 270 mm x 50 mm bands and intermediate 250 mm x 25 mm were cut from the 5320-1 prepreg roll. The large bands were placed on vacuum bag films in order to prevent resin flow on the fixture platens. The extremity of the intermediate sample that will be pulled by the MTS machine was also partially covered with a film to protect the tensile test fixture jaws (Figure 7 b)). The pulling speed was fixed at 20 mm/min and the contact area was 2500 mm^2, as the width of the sample was fixed at 25 mm and the contact length at 100 mm. Six experiments were conducted to measure the coefficient of friction of the prepreg at three different temperatures (50, 70 and 120 °C) and two normal forces (266 and 533 N). The testing temperature was set at 50°C, 70°C and 120°C, in order to investigate friction with high (50°C), intermediate (70°C) and low (120°C) resin viscosity. A total of six samples were tested per condition.

Figure 8 shows the average measured peak force as a function of normal force for the tested temperatures. Linear regression was fitted to the data, the slope and intercept values obtained are shown on the chart. Using the corresponding resin viscosity at a given temperature, the contact area and the pulling speed, the resin film thickness was calculated from the intercept values. As expected, the intercept is decreasing with increasing temperature, as the viscosity is getting lower. The resin film is also getting thinner at higher temperature and lower viscosity. This makes sense, as a more fluid resin will flow under the pressure at the contact platens. The friction coefficient slightly decreases with temperature. Nevertheless, it is difficult to confirm this trend due to experimental errors. The mean value of the inter-ply friction for the Cycom 5320-1 is 0.11 under the test conditions, with an average variation of 8.94%.

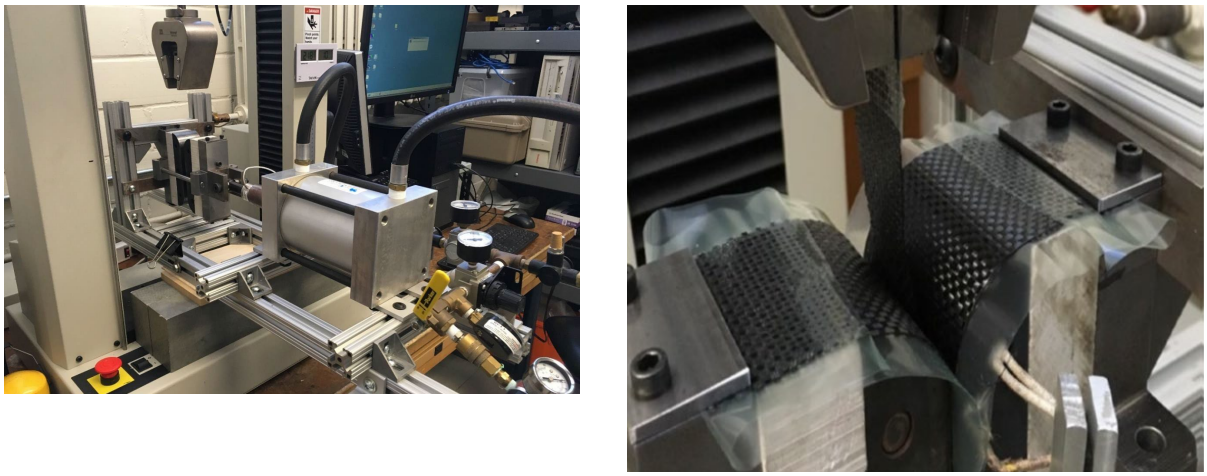

a) b)

Figure 7 a) Friction fixture mounted on the MTS machine, b) Prepreg samples installed on the friction fixture to be tested.

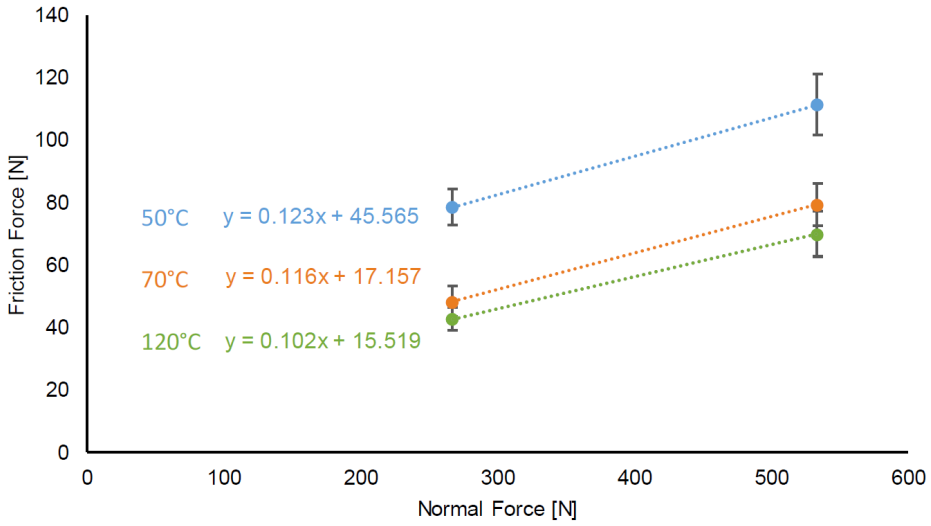

Figure 8 Cycom 5320-1 friction tests results. The error bars correspond to the standard deviation of a set of measurement.

3. CORE CRUSH MODEL

A key goal of this model is to predict core crush as a result of various geometric, material, and processing parameters. In practice, parts which exhibit any degree of core crush are considered failed and are scrapped. Therefore, this model seeks only to predict the *onset* of the core-crush event and not its magnitude. The finite element model is built using ABAQUS\Standard 2019.

First, the core pressure developed by Kratz [17] was used to investigate the evolution of core pressure with the measured skin permeability reported in Section 2.1. Core pressure simulations were performed for the following conditions for a thin skin thickness. Severe conditions were simulated where an initial core pressure of 50 kPa was used to assume incomplete core evacuation before the start of the temperature ramp. The initial core moisture content was set to 4% to represent a high moisture equilibrium at 50% relative humidity. Nominal conditions were also simulated with an initial core pressure of 5kPa and initial moisture content of 0.5% for a fully evacuated dry core.

For the transverse evacuation scenario, the air can flow through the skin thickness. For the in-plane evacuation scenario, the air flows through the edge band breathing system. The severe scenario lead to significant core pressure increase (peak from 80-250 kPa) particularly for the in-plane evacuation scenario. The pressure peak occurs at minimum resin viscosity. The nominal scenario however shows insignificant pressure peaks with a maximum value of 30 kPa. Although, core pressure was shown to have a significant effect on core crush [18], it is believed that unless the internal pressure can be precisely controlled to a desired value, a conservative approach of neglecting core pressure in the crush onset simulation is a preferred approach. Thus, the following core crush model development neglects internal core pressure effects.

3.1 Model components and geometry

The core crush model contains three parts, the top and bottom fibre reinforced polymer skins and the honeycomb, as shown in Figure 9. The honeycomb core is modelled using an equivalent solid mesh (ESM). Bag and tool plate are not modelled. A 2.5D model is used to represent the core crush problem, with geometry parameters shown in Figure 10 that are required by the script to generate the model. Actual Part Depth is the depth of the entire part, which is assumed to be very long. The geometry value *Part Depth* is set simply to maintain a convenient mesh aspect ratio and density which captures Poisson's effects accurately, an important factor in honeycomb cores. This assumes that the represented part has a high aspect ratio (i.e. Centre Length >> Actual Part Depth).

3.2 Mesh

There are several test methods and modelling algorithms developed to model uncured prepreg [19-22]. A key observation is that a classical shell mesh (continuum or continuum solid shell) is insufficient for modelling the non-linear deformation of uncured prepregs. In this application, since onset of displacement is considered, non-linearities associated with large displacements are not relevant. Since this work is limited to small-deformations, continuum solid shell theory is assumed to suffice. The top and bottom skins are meshed using SC8R continuum solid shell elements with second order accuracy and hourglass control enabled to prevent excessive distortion. The default mesh size for the skin is a function of the minimum of either the part depth or the core height, the minimum number of elements per edge, and the additional element density factor. The mesh size is curvature controlled automatically in Abaqus. The core is meshed using C3D8HS linear brick elements with hybrid formulation (constant pressure) and improved surface stress visualization. An advancing front algorithm using the sweep technique is used to generate the mesh. The default mesh size is calculated with an additional term as the core is to be finer than the skin. The core too has a curvature-controlled mesh.

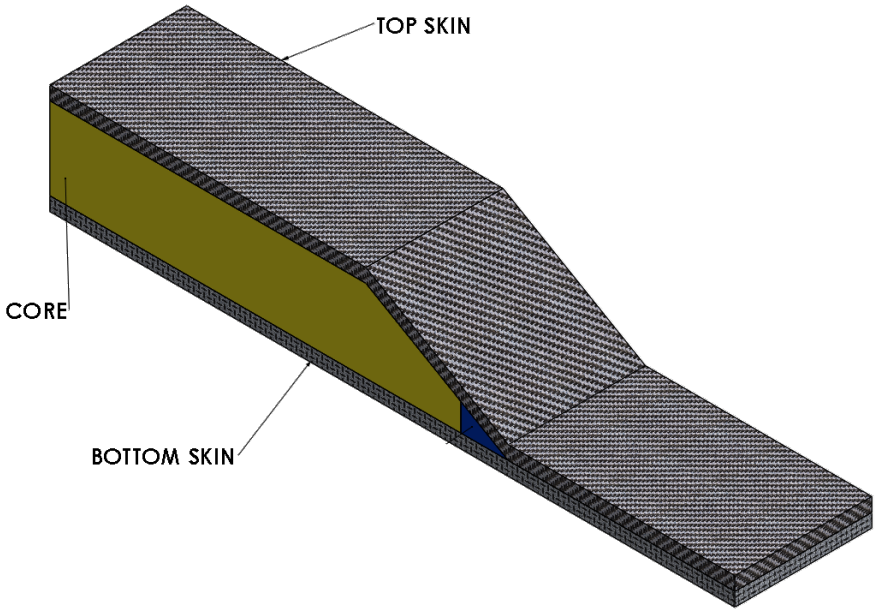

Figure 9 Core crush system.

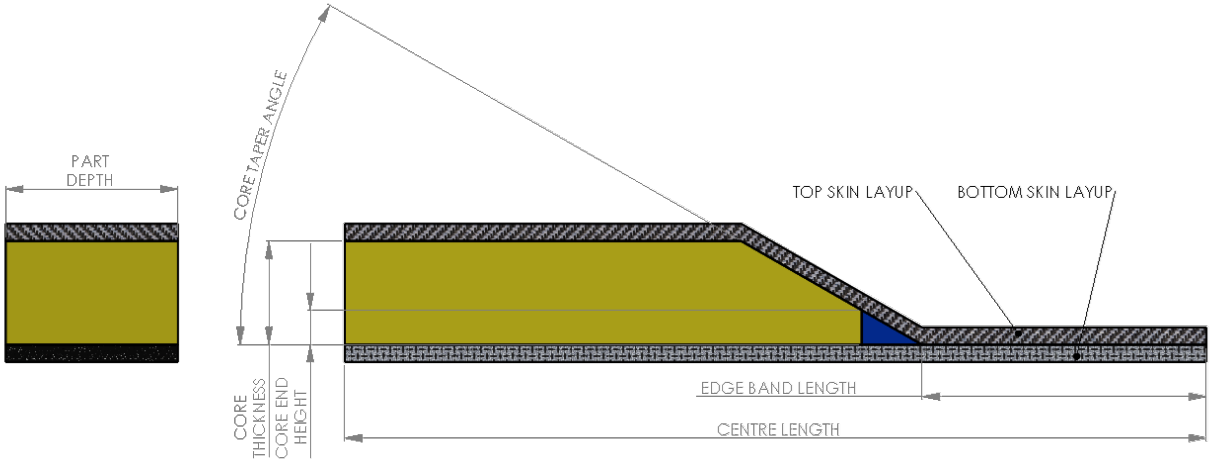

Figure 10 Model geometry parameters.

3.3 Boundary Conditions

All nodes which lie on faces normal to the Z axis are prevented from translation in the Z direction. This approximates an infinite part depth and thus a plane-strain problem. The geometric definition of part depth ensures that element aspect ratios are respected, and that Poisson's effects are captured in the model. This boundary condition is applied to the core, top skin, and bottom skin. All nodes which lie on the end face, which is normal to the X (1st) axis are prevented from translation in the X direction. This includes three surfaces, one each on the top skin, bottom skin, and core. The top face of the bottom skin which contacts the core, and top skin is blocked from translation in all directions. All motion is measured as "relative" to this face. This assumes that

there is significant tool-part interaction relative to other frictional loads as well as no out-of-plane distortion of the bottom skin.

3.4 Material Properties

Skin material properties – as well as the friction and cohesive interactions which are dependent on the resin – are degree of cure (DoC) dependent. The developed model includes the ability to linearly ramp the DoC from 0.0 to some user prescribed DoC value. For this work, it is assumed that *during the crush event the degree of cure properties remain constant*. The core-crush phenomenon is due to a collapse [14] and thus occurs rapidly. Therefore, this assumption states that insignificant cure will happen during this near instantaneous crush event. The prepreg skin elastic response is a function of the degree of cure of the resin. Per the experiments of Thorpe [23], it can be said that the elastic response – shown with the storage modulus, G' – is dominated by the fibre bed behaviour which is DoC independent. In the sample, the prepreg modulus only changes as the matrix vitrifies. Consolidation pressure is applied before vitrification, and thus the crush event will occur before vitrification. Therefore, it can be assumed that the skin modulus is constant during the crush event and DoC independent. The skin Young's modulus is assumed to be 5 GPa from the bi-material beam measurements done by Thorpe [23].

3.5 Interactions

Between the two skins, a friction coefficient is defined using the Finite Sliding formulation. The skins can freely separate from one another but cannot translate through each other. The friction coefficient is assumed to be pressure and temperature independent. A cohesive interaction is applied between the core and skins with the Small Sliding contact formulation. There is no stiffness in the out-of-plane direction ($K_{nn} = 0.0$), which means the skins and core are free to separate. The in-plane stiffness is calculated as a function of relative contact area and the modulus of the fibre bed. The maximum out-of-plane stress is set to 10^{-6} MPa and the in-plane stress to 1000 MPa with the goal of allowing no out-of-plane stress and infinite in-plane stress.

3.6 Loads

The only external load in the model is the autoclave pressure, which is applied as a pressure load to the top surface of the top skin. This, along with the X and Z boundary conditions applied above, allows deformation and translation of the top skin in the X and Y directions. This allows the possibility of skin wrinkling, which may have an impact on how the pressure is distributed to the core.

4. RESULTS

The full experimental batteries performed by Aurora and Boeing were run in both the 1 & 2 directions for the core to evaluate the accuracy of the finite element model. The crush event is predicted using a safety factor (SF), as calculated in Equations 2-4. The two stresses used to calculate safety factor are the maximum stress in the core, as well as the mean stress in the taper region as shown in Figure 11. Crush is defined when the safety factor calculated is less than the

target. Accuracy is calculated as the ratio of correct predictions (i.e. no crush predicted in FEA & no crush experimentally observed), as calculated in Equation 5.

$$SF_{max} = \frac{\sigma_{Yield}}{\sigma_{11,\ Max\ Compressive,\ Core}} \quad [2]$$

$$SF_{Mean} = \frac{\sigma_{Yield}}{\sigma_{11,\ Mean,Taper}} \quad [3]$$

$$\begin{cases} Crush \textbf{ if } SF < SF_{Target} \\ No\ Crush \textbf{ if } SF > SF_{Target} \end{cases} \rightarrow Typical\ SF_{Target} = 1 \quad [4]$$

$$Accuracy = \frac{\#\ of\ Correct\ Predictions}{\#\ of\ Tests} * 100\% \quad [5]$$

The crush event can be said to occur in either two cases, which are shown in Figure 12, with yielded regions ($\sigma > \sigma_{Yield}$) marked in grey. The first, Case (A), occurs when only points on or near the core surface exceed the yield stress. These large local maximum stresses indicate local yielding, which predicts unstable collapse of the core if surface properties are the same as that of the bulk core material as assumed. Surface stresses are sensitive to the interaction between the skin and core. Case (A) is represented using maximum stress. The second case, Case (B), is when the yield stress is exceeded through the thickness of the core, which will certainly cause unstable collapse. The through thickness distribution of this stress indicates this core is likely to fail regardless of surface effects. Case (B) is represented using the mean stress in the taper region.

The crush results for a range of safety factors using both the mean and maximum stresses are shown in Figure 13. As safety factor increases, accuracy of stabilized case prediction tends to decrease. Max stress is shown to be more accurate for unstabilized cases, which indicates the assumption of material homogeneity is accurate for unstabilized cores. The stabilized core is more accurately predicted using mean stress, indicating that surface stress is not predictive of failure for stabilized cases. The inaccuracy of surface stress is likely related to the fact that the core is modelled homogenously when the stabilization process is a surface treatment. Mean stress reduces the influence of high surface stresses and requires global yielding, which appears to be a more accurate predictor for stabilized core. No consistent relationship between safety factor and accuracy is observed, so a typical safety factor of 1, for which there is 81% accuracy is used for subsequent evaluation.

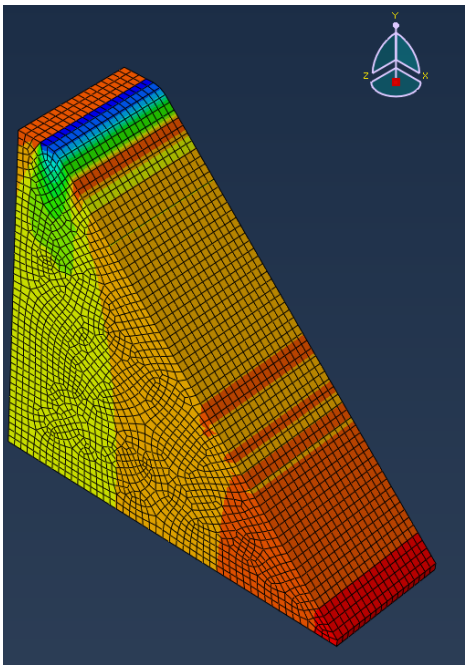

Figure 11 Taper Region used to calculate mean stress.

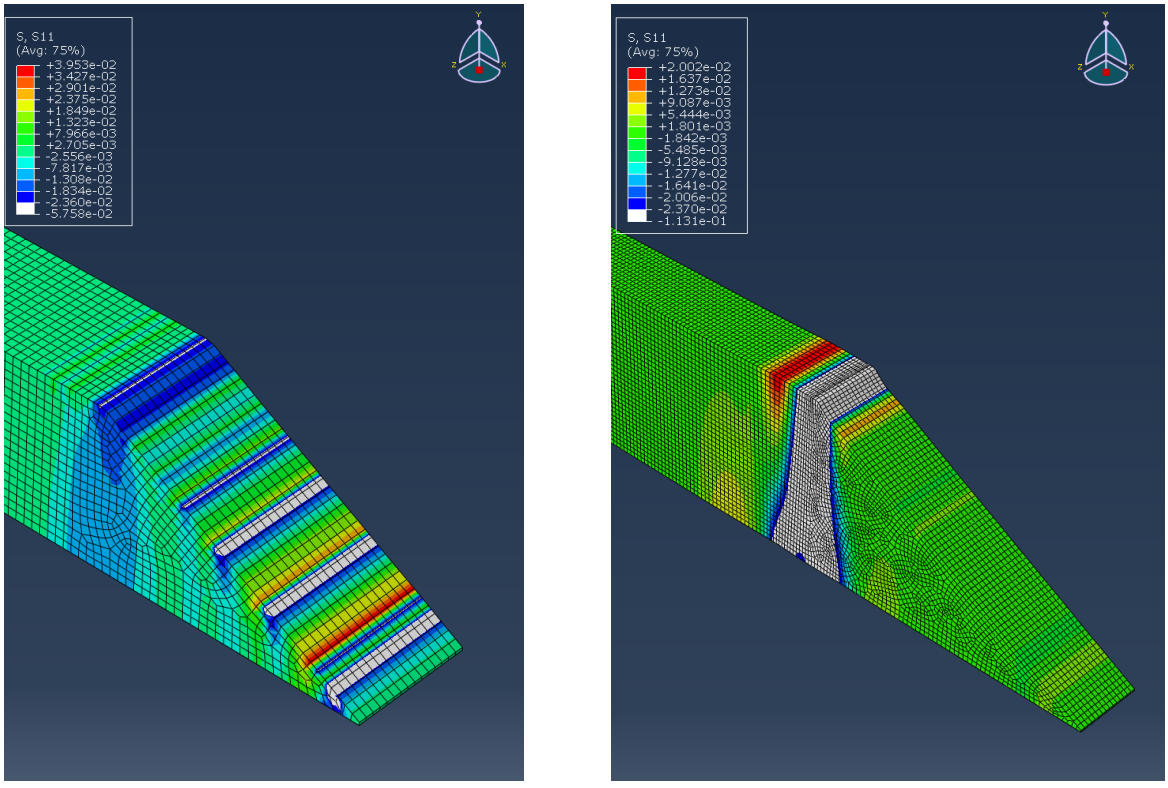

a) b)

Figure 12 a) Local yield and b) global yield regimes for core crush, yielded regions shown in grey

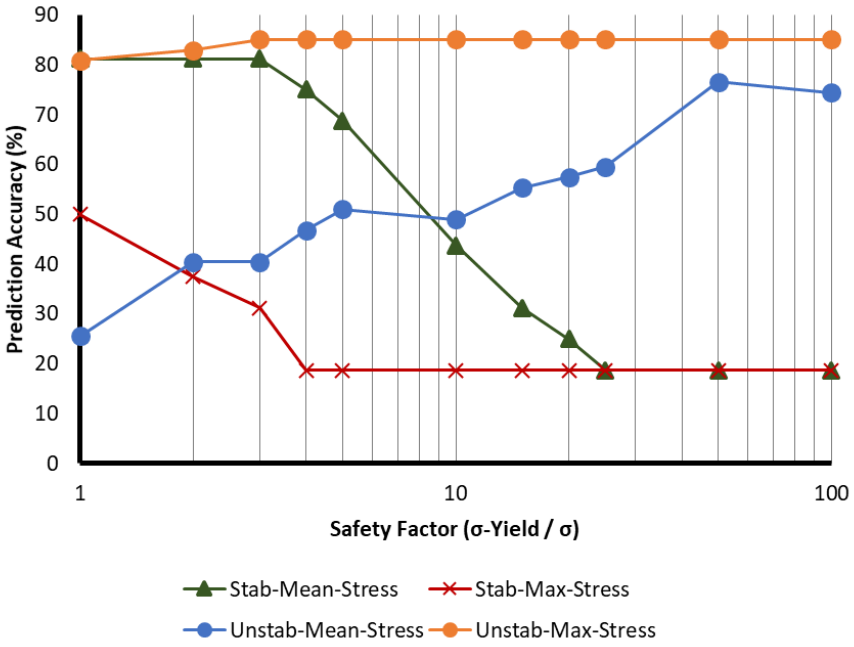

Figure 13 Taper region used to calculate mean stress.

The cases of interest are those which are incorrectly predicted by the model. Addressing first unstabilized cases which do not match experiments, the margins of incorrect prediction tend to be quite close. In fact, for some cases, crush is predicted in one direction but not the other. Similar observations arise when looking at the stabilized cases, where safety factors are close to 0.2. The closeness of incorrect predictions to correctness for both stabilized and unstabilized cases indicate sensitivity to assumptions and sources of error. Key assumptions made in the development of this model are the homogeneity of the core material properties, omission of tool-part interactions and bag effects, as well as the lack of interply modelling. The skin properties are also estimated, significant further development is needed especially given the complexity of their uncoupled tensile, bending, and compression behaviours. Despite these known sources of error, the model captures major influencing factors and can predict with 81% accuracy the onset of core crush.

5. CONCLUSION

The following statements summarize the main findings form this work:

1) Skin air permeability was measured with a specialized fixture. Average values for in-plane and transverse permeability were obtained for Cycom 5320-1, transverse: 1.60×10^{-17} m^2, in-plane: 2.96×10^{-14} m^2 and Hexcel 8552-1, transverse: 1.19×10^{-17} m^2, in-plane: 2.35×10^{-14} m^2.
2) Prepreg-prepreg friction was measured at 0.11 for Cycom 5320-1.
3) Honeycomb core in-plane compression was measured: unstabilized core modulus and yield stress ranges from 0.04-0.147 MPa and 0.012-0.029 MPa respectively. Stabilized core modulus and yield stress ranges from 1.47-15.5 MPa and 0.118-0.610 MPa respectively.

4) A core pressure model was used to estimate the core pressure during cure. In conditions if poor core evacuation and high core moisture content, peak pressure of 80-250 kPa are predicted, while in condition of good core evacuation and low moisture content, core peak pressure was below 30 kPa.
5) A FEA core crush model was developed with a prediction accuracy of 81%.

6. ACKNOWLEDGMENTS

The authors would like to acknowledge Geoff Butler from Boeing for his contribution to the core crush simulation trials. Special thanks to Gary Wolfe from Aurora for the core crush validation experiments and material donation for the 8552-1 honeycomb panels. The authors would like to acknowledge the funding from Boeing for this project with NASA under award No. NNL09AA00A and 80LARC17C0004.

7. REFERENCES

[1] C. Martin, J. Seferis, and M. Wilhelm, "Frictional resistance of thermoset prepregs and its influence on honeycomb composite processing," *Compos. Part Appl. Sci. Manuf.*, vol. 27, no. 10, pp. 943–951, 1996.
[2] F. U. Buehler, J. C. Seferis, and Z. SHANYING, "Consistency evaluation of a qualified glass fiber prepreg system," *J. Adv. Mater.*, vol. 33, no. 2, pp. 41–50, 2001.
[3] C. Martin, J. Putnam, B. Hayes, J. Seferis, M. Turner, and G. Green, "Effect of impregnation conditions on prepreg properties and honeycomb core crush," *Polym. Compos.*, vol. 18, no. 1, pp. 90–99, 1997.
[4] H. Hsiao, S. Lee, and R. Buyny, "Core Crush Mechanisms and Solutions in the Manufacturing of Sandwich Structures," in *Recent Advances in Experimental Mechanics*, Springer, 2002, pp. 689–700.
[5] "Subcommittee D30.09 : Published standards under D30.09 jurisdiction." [Online]. Available: https://www.astm.org/COMMIT/SUBCOMMIT/D3009.htm. [Accessed: 01-Aug-2019].
[6] Gibson L. J., Ashby Michael Farries, Schajer G. S., and Robertson C. I., "The mechanics of two-dimensional cellular materials," *Proc. R. Soc. Lond. Math. Phys. Sci.*, vol. 382, no. 1782, pp. 25–42, Jul. 1982.
[7] J. Zhang and M. F. Ashby, "The out-of-plane properties of honeycombs," *Int. J. Mech. Sci.*, vol. 34, no. 6, pp. 475–489, Jun. 1992.
[8] R. Roy, S.-J. Park, J.-H. Kweon, and J.-H. Choi, "Characterization of Nomex honeycomb core constituent material mechanical properties," *Compos. Struct.*, vol. 117, pp. 255–266, Nov. 2014.
[9] D. Ruan, G. Lu, B. Wang, and T. X. Yu, "In-plane dynamic crushing of honeycombs—a finite element study," *Int. J. Impact Eng.*, vol. 28, no. 2, pp. 161–182, Feb. 2003.
[10] A. Hönig and W. J. Stronge, "In-plane dynamic crushing of honeycomb. Part II: application to impact," *Int. J. Mech. Sci.*, vol. 44, no. 8, pp. 1697–1714, Aug. 2002.
[11] Z. Zheng, J. Yu, and J. Li, "Dynamic crushing of 2D cellular structures: A finite element study," *Int. J. Impact Eng.*, vol. 32, no. 1, pp. 650–664, Dec. 2005.

[12] G. B. Chai and S. Zhu, “A review of low-velocity impact on sandwich structures,” *Proc. Inst. Mech. Eng. Part J. Mater. Des. Appl.*, vol. 225, no. 4, pp. 207–230, Oct. 2011.
[13] B. L. Buitrago, C. Santiuste, S. Sánchez-Sáez, E. Barbero, and C. Navarro, “Modelling of composite sandwich structures with honeycomb core subjected to high-velocity impact,” *Compos. Struct.*, vol. 92, no. 9, pp. 2090–2096, Aug. 2010.
[14] D. Mohr and M. Doyoyo, “Large plastic deformation of metallic honeycomb: orthotropic rate-independent constitutive model,” *Int. J. Solids Struct.*, vol. 41, no. 16, pp. 4435–4456, Aug. 2004.
[15] “COMPRO Model Documentation, Release 1.5.9.” Convergent Manufacturing Technologies Inc., 10-Jul-2017.
[16] P. Hubert, T. Centea, L. Grunefelder, S. Nutt, J. Kratz, and A. Levy, “2.4 Out-of-Autoclave Prepreg Processing,” in *Comprehensive Composite Materials II*, Oxford: Elsevier, 2018, pp. 63–94.
[17] J. Kratz and P. Hubert, “Vacuum bag only co-bonding prepreg skins to aramid honeycomb core. Part I. Model and material properties for core pressure during processing,” *Compos. Part Appl. Sci. Manuf.*, vol. 72, pp. 228–238, 2015.
[18] D.J. Renn, T. Tulleau, J.C. Seferis, R.N. Curran and K.J.J. Ahn, "Composite Honeycomb Core Crush in Relation to Internal Pressure Measurement", Adv. Mater. 1995, 21, 31.
[19] B. Liang, N. Hamila, M. Peillon, and P. Boisse, “Analysis of thermoplastic prepreg bending stiffness during manufacturing and of its influence on wrinkling simulations,” *Compos. Part Appl. Sci. Manuf.*, vol. 67, pp. 111–122, Dec. 2014.
[20] H. Alshahrani and M. Hojjati, “Bending behavior of multilayered textile composite prepregs: Experiment and finite element modeling,” *Mater. Des.*, vol. 124, pp. 211–224, Jun. 2017.
[21] Y. Larberg and M. Åkermo, “In-plane deformation of multi-layered unidirectional thermoset prepreg – Modelling and experimental verification,” *Compos. Part Appl. Sci. Manuf.*, vol. 56, pp. 203–212, Jan. 2014.
[22] H. Alshahrani and M. Hojjati, “A theoretical model with experimental verification for bending stiffness of thermosetting prepreg during forming process,” *Compos. Struct.*, vol. 166, pp. 136–145, Apr. 2017.
[23] R. J. Thorpe, “Experimental characterization of the viscoelastic behavior of a curing epoxy matrix composite from pre-gelation to full cure,” University of British Columbia, 2013.